Tailoring electronic configurations in adsorptive sites for the enhancement of As(V) removal from groundwater

Kaixun Tian, Jing Xiao, Jian Shen and He Zhao

ABSTRACT

In the past few decades, heavy metal pollution, such as As(V), has become an important issue for aqueous environment safety. For reasons of practical feasibility and cost-effectiveness, adsorption has been widely used in the water treatment and reuse community, with rapid development of adsorbents. However, the precise control of the electronic configuration of the adsorbents' sites to enhance adsorption performance is largely unexplored. In this study, to demonstrate the effect of electronic configuration on adsorption performance, we synthesized granular activated carbon (GAC) supported Fe-based hydroxides adsorbents by varying the valence state in transition metals. Furthermore, the adsorbents are characterized by X-ray photoelectron spectroscopy (XPS), Fourier transform infrared spectroscopy (FT-IR), and scanning electron microscopy (SEM) to identify surface structure and morphological properties. Adsorptive performance studies show that the adsorption capacity and arsenic removal efficiency of Fe(II)-GAC are twice those of Fe(III)-GAC, as a matter of charge transfer between adsorbents and cationic pollution (such as Fe-O and As species). Finally, PO_4^{3-} was selected as a control sample to confirm the rationality of the removal mechanism. Collectively, fine-tuning of the electronic configuration from charge transfer will not only benefit heavy metal removal channels, but also supply fundamental information for adsorbents design for organics removal.

Key words | adsorption, arsenic (V) removal, electronic configurations, iron oxide hydrate

Kaixun Tian
Jing Xiao
Jian Shen (corresponding author)
Department of Environment and Resources,
Hunan Engineering Laboratory for Complex Heavy Metal Wastewater Purification and Application Technology,
Xiangtan University,
Xiangtan 411105,
China
E-mail: *js_xtuhzy@xtu.edu.cn*

He Zhao
Beijing Engineering Research Center of Process Pollution Control, Division of Environment Technology and Engineering, Key Laboratory of Green Process and Engineering,
Institute of Process Engineering, Chinese Academy of Sciences,
Beijing 100190,
China

INTRODUCTION

Recently, rapid growth of industrialization and urbanization have produced significant problems of various toxic heavy metals pollution. In particular As(V) exists at high concentrations in anaerobic groundwater, inducing carcinogenicity, illness, and disability. Due to the environmental toxicity of arsenic, many countries and organizations must enforce stricter limits as a matter of urgency (Council of the European Union 1998; U.S.EPA 2002; Ministry of Health of the P.R. China 2006; WHO 2011).

To meet such requirements, conventional pollution control technologies, such as precipitation-coagulation, membrane separation, ion exchange and adsorption (Cui *et al.* 2015; Jaiswal *et al.* 2018; Kartinen & Martin 1995; Naeem *et al.* 2006; Naeem *et al.* 2009a; Naeem *et al.* 2009b), are being developed or greatly improved. However, considering economic factors and technological feasibility, adsorption is still the most promising choice for treatment of As-containing wastewater (Fox *et al.* 2016; Li *et al.* 2010). For example, 'ferrihydrite process' based adsorption, developed by U.S.EPA (2002), helps to considerably decrease high As(V)-concentrations down to 100 mg/L. Presently, novel adsorbents include activated carbon, polymeric hybrids, natural minerals and transition metal oxides (McNeill & Edwards 1997), which are being developed due to the need for effective adsorbents. Among the above adsorbents, iron-based adsorbents have attracted more attention in treating As-containing wastewater owing to the strong affinity between iron/iron oxides and arsenic compounds,

doi: 10.2166/ws.2019.197

high isoelectric points and specific surface area, especially for hydrated ferric oxide (HFO) (Li *et al.* 2016; Yan *et al.* 2018). However, HFO is generally perceived as amorphous and suspended in solution, causing difficulties in solid-liquid separation. To resolve this problem, HFOs are often grown on a porous matrix, such as a strong-acid cation-exchange resin, carbon black (Cumbal & Sengupta 2005; Pan *et al.* 2010; Jing *et al.* 2011). However, few reports focus on the effects of interface properties on the arsenate adsorption performance, especially electronic configuration of adsorptive sites in HFO and charge transfer pathways between HFO and the matrix.

Therefore, the motivation for this work is to synthesize composite adsorbents, namely hydrated ferric oxide-granular activated carbon composites, to investigate the effects of electronic configuration of active sites on As removal efficiency. As(V) removal performances were evaluated by considering dosage and pH effects. Furthermore, the possible adsorptive mechanisms were highlighted via analyzing experimental data with scanning electron microscope (SEM) images, Fourier transform infrared spectrum (FT-IR), X-ray diffraction (XRD) patterns, X-ray photoelectron spectroscopy (XPS) and Brunauer-Emmett-Teller (BET). Additionally, an interfering ion, PO_4^{3-} is also introduced as a feedback to double-check the validity of the plausible mechanism.

MATERIAL AND METHODS

Materials

All chemicals used were purchased from Aladdin without further purification, except for granular activated carbon (GAC). The As(V) stock solution with the concentration of 100.0 mg/L was prepared by dissolving sodium arsenate (Na_3AsO_4•$12H_2O$, 99%) in DI water. The purchased GAC with a density of 0.45–0.55 g/cm^3 was first soaked in 10% nitric acid for 24 hours, then ultrasonicated for another 15 minutes. Finally, the samples were washed with DI water until the pH of the supernatant was close to 7.0, and then dried at 378 K. The as-prepared GAC was kept in a drying cabinet for future use.

Adsorbents preparations

In this work, iron oxide-coated granular activated carbon (Fe-GAC) with different valence states were mainly prepared according to previous recipes (Gu *et al.* 2005; Jang *et al.* 2008; Yan *et al.* 2011). The modified procedures are as below.

Fe(III)-GAC: Firstly, the GAC was dispersed in ferric chloride solution with the concentration of 1.5 mol/L. Secondly, the mixtures were stirred for 24 hours at 298 ± 1 K in order to make the $FeCl_3$ fully immersed in the GAC. After that, the solution pH was adjusted to the 7.0–8.0 range by 0.1 M NaOH in order to fabricate the fresh metal (hydro) oxide. Finally, the pristine samples were washed with DI water several times and dried at 373 K for 4 hours. This adsorbent was labeled as Fe(III)-GAC.

Fe(II)-GAC: Firstly, the GAC was dispersed in ferrous chloride solution with the concentration of 1.5 mol/L under nitrogen protection. Next, the pH of the solution was controlled at 4.5–5.0 by 0.1 M NaOH to convert the metal salt to metal (hydro)oxide. Finally the as-prepared Fe(II)-GAC was washed with DI water several times and dried at 373 K for 4 hours. The sample was labeled as Fe(II)-GAC.

Characterizations

The prepared Fe-GAC samples were examined by a scanning electron microscope (SEM) (JSM-5600LV) for the surface morphology check. X-ray diffraction (XRD) patterns were used to characterize crystal structure using a D8-ADVANCE X-ray powder diffractometer (Bruker AXS, Germany) under Cu Kα radiation, equipped with Sol-X detector and operated at 50 kV and 100 mA with a scanning speed of 2° min^{-1} over the range $10° < 2\theta < 80°$. The surface functional groups of the samples were recorded by a Fourier transform infrared (FT-IR) spectrophotometer from 400–4,000 cm^{-1} (NICOLET-380, Nicolet precision instruments, USA). The surface chemical composition of the samples was examined by X-ray photoelectron spectroscopy (XPS) (ESCALAB 250 X-ray Photoelectron Spectrometer, Thermo Fisher Scientific Inc., USA) with an Al Kα anode (1,486.6 eV photon energy, 0.05 eV photon energy resolution, 150 W). The BET/BJH surface area of the samples was measured by N_2 adsorption/desorption isotherm with

NOVA1000e Series Surface Area and Pore Size Analyzers (Quantachrome Instruments, USA).

Adsorption performance

The adsorption performance was evaluated by considering dosage and pH effects. In our experiments, a certain amount of adsorbent is added into 20 ml 20 mg/L arsenate solution with solution pH ranging from 3.0 to 12.0. Then the mixture is shaken in a vapor-bathing vibrator at 298 K for 8 hours with a stirring velocity of 125 rpm/min. After that, the sample is filtered using a 0.45 μm filter membrane and the suspension is measured by hydride generation atomic fluorescence spectrometry to calculate the amounts of adsorbed arsenic. Additionally, with the same methods, PO_4^{3-} was introduced as a competitive ion to confirm the adsorptive mechanism under the optimal conditions for As(V) removal.

RESULTS AND DISCUSSION

Morphology and structural characterizations

Firstly, the SEM images (Figure 1(a)) show that the surface of the GAC displays a porous structure with the surface area of 427.580 m^2/g (Table 1). However, the surface morphology becomes rougher as the Fe valence state increases from +2 to +3 (Figure 1(a)). Meanwhile, Table 1 shows that the surface areas decrease from 427.580 to 330.765 m^2/g and 219.684 m^2/g. Therefore, it infers that Fe species show epitaxial growth on the GAC surface. Moreover, compared with GAC, the XRD patterns (Figure 1(b)) for both Fe(II)-GAC and Fe(III)-GAC show that there is no characteristic peak of the Fe species except for the GAC peak, which is ascribed to the HFO amorphous structure (Gu *et al.* 2005). Therefore, in order to further identity the HFO structure, FT-IR and XPS are used. Looking at the FT-IR spectrum (Figure 1(c)), the peak with 1,118 cm^{-1} of Fe(II)-GAC was assigned to Fe-OH. Fe-O stretching in Fe(II)-GAC leads to absorptive signals at 794 cm^{-1} and 890 cm^{-1}. For Fe(III)-GAC, the peak at 472 cm^{-1} found in the FT-IR spectrum originated from the Fe-O stretching peak. Furthermore, compared with pure GAC in the C1s spectrum, the composite adsorbents contain C*-O-Metal and C*-O (Figure S1, Supplementary Material) (C* denotes a carbon atom interacting with an oxygen atom in HFO), except for C species, which indicates that HFO are immobilized by GAC via C-O band formation. To further investigate the slight difference in GAC, Fe(II)-GAC and Fe(III)-GAC, we put more emphasis on the peak shift for C1s and Fe2p binding energy (Figure 1(d) and 1(e)). It is common sense that the peak of binding energy for Fe(II)-GAC is lower than that for Fe(III)-GAC, which means greater electron density in Fe(II)-GAC. This result can be easily explained by the fact that six 3d electrons exist in the outmost layer in Fe(II), while the number of electrons in the corresponding part is five in the Fe(III)-GAC structure. However, in the C1s spectrum, the C1s peak shows a red shift for Fe(II)-GAC and Fe(III)-GAC, compared with pure GAC, which means that the charge density of elemental carbon may be enhanced after supporting HFO. As Figure S1 indicates, C species exist in the form of C, O-C, and C-C. Due to the high electronegativity of the O atom, the charge in the C* atom shows a transfer tendency from C* to O, resulting in a charge transfer from neighbor C, denoted as C_n, to the C* atom. Actually, the binding energy of O-C* is lower than that of Cn-C*, indicating the net charge density enhancement of C*. Therefore, compared with GAC, the increase of charge density of the C* atom due to the high electronegativity of the O atom, will result in C1s spectrum red shift. To further confirm this hypothesis, we also show the contrast between Fe(II)-GAC and Fe(III)-GAC in the C1s spectrum. It is known that the arrangement of electrons in the outermost layer of atoms of Fe(II) and Fe(III) is $3d^6$ and $3d^5$, respectively. According to the Hund rule, due to its half-filled state, all d electrons tend to keep single spin state, which means that d orbits do not easily accept or donate electrons. However, for Fe(II), due to the high electronegativity of the O atom, one anti-spin electron could be inspired from d orbits in order to minimize the total energy. On this occasion, the charge density improvement of O in Fe-O will come from the electron in the outermost layer, without the aid of charge transfer from C_n. Therefore, for Fe(III)-GAC, the charge density of C* will be more than that of Fe(II)-GAC, resulting in a further slight red shift of the C1s spectrum. Hence, the interaction between the matrix and HFO is rooted in charge transfer.

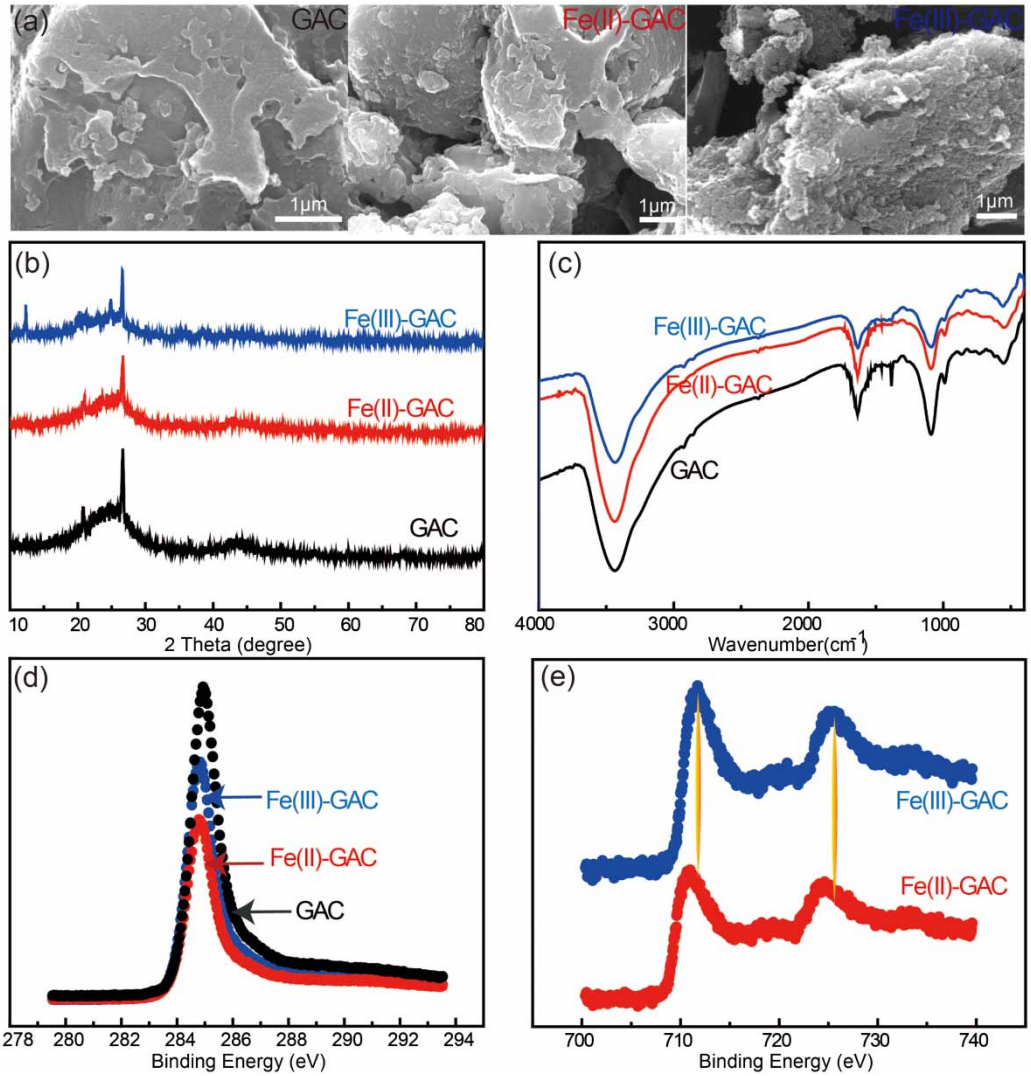

Figure 1 | (a) Scanning electron microscope (SEM) images of pure granular activated carbon (GAC), granular activated carbon supported hydrated ferric oxide with Fe(II), and granular activated carbon supported hydrated ferric oxide with Fe(III) from left to right. (b) X-ray diffraction spectrums (XRD) of pure granular activated carbon (GAC), granular activated carbon supported hydrated ferric oxide (Fe(II)), and granular activated carbon supported hydrated ferric oxide (Fe(III)) with a scanning speed of 2° min^{-1} over the range $10^{\circ} < 2\theta < 80^{\circ}$. (c) Spectrums of Fourier transform infrared (FT-IR) of pure granular activated carbon (GAC), granular activated carbon supported hydrated ferric oxide (Fe(II)), and granular activated carbon supported hydrated ferric oxide (Fe(III)) from 400–4,000 cm^{-1}. (d) X-ray photoelectron spectroscopy (XPS) C1s spectrums of pure granular activated carbon (GAC), granular activated carbon supported hydrated ferric oxide (Fe(II)), and granular activated carbon supported hydrated ferric oxide (Fe(III)) with an Al Kα anode (1,486.6 eV photon energy, 0.05 eV photon energy resolution, 150 W). (e) X-ray photoelectron spectroscopy (XPS) Fe2p spectrums of granular activated carbon supported hydrated ferric oxide (Fe(II)) and granular activated carbon supported hydrated ferric oxide (Fe(III)) with an Al Kα anode (1,486.6 eV photon energy, 0.05 eV photon energy resolution, 150 W).

Table 1 | Pore volume distributions and surface areas of GAC, Fe(II)-GAC and Fe(III)-GAC

Sample	BET surface area (m^2/g)	BJH surface area (m^2/g)	BJH desorption pore volume (cc/g)	BJH average pore diameter (nm)
GAC	427.580	241.725	0.194	1.364
Fe(II)-GAC	330.765	218.295	0.179	1.138
Fe(III)-GAC	219.684	126.778	0.095	1.350

Adsorption performance

Generally, the surface charge and the quantities of intrinsic absorptive sites are key factors influencing adsorptive performances. In practice, the factors could be controlled by varying dosage and pH values. Therefore, the adsorption performance of composite adsorbents was assessed by

investigating dosage and pH effects. The dosage effect was first investigated by tuning adsorbent addition concentration from 0.1 mol/L to 1.2 mol/L as Fe calculation within 20 mg/L As(V) at pH 7.0. Figure 2(a) and 2(c) show that the As(V) removal efficiency increased with increased Fe(II)-GAC or Fe(III)-GAC addition. The best performance of both adsorbents was achieved at the same point, namely, at a dosage of 0.8 mol/L. At 0.8 mol/L or above, both As(V) removal rates reached a plateau. Therefore, we set 0.8 mol/L as the optimal dosage for further investigation. The optimal As(V) removal rates over Fe(II)-GAC and Fe(III)-GAC materials are 95.84% and 47.40% with a dosage of 0.8 mol/L at pH 7, respectively. Furthermore, it is known that pH can tune Fe species, surface charge type, and surface charge amounts, and also that the optimal pH should theoretically be around the point of zero charge (PZC) due to charge neutralization (Kam & Gregory 2001; Yuan *et al.* 2019) because suspension particles destabilization takes place over the PZC if only dependent on the role of charge neutralization (Shen *et al.* 2014). As previous data indicated, the PZC of Fe(III)-GAC (8.4) (Hu *et al.* 2004) is higher than that of Fe(II)-GAC (5.8) (Chowdhury & Yanful 2010). Therefore, the performance of Fe(III)-GAC should be superior to that of Fe(II)-GAC if the pH is more than 5.8. Actually, the investigation results of pH effects are beyond our expectation. In Figure 2(b), for Fe(III)-GAC, the effects of pH on As(V) removal efficiency and adsorption capacity mainly comply with charge neutralization because of the optimal pH in the vicinity of PZC. However, for Fe(II)-GAC (Figure 2(d)), although the optimal pH is 5.0, which is close to the PZC, the As(V) removal efficiency and adsorption capacity of Fe(II)-GAC are still higher than that of Fe(III)-GAC, and it also keeps a stable level (As(V) removal efficiency of 90% and above) with a wider

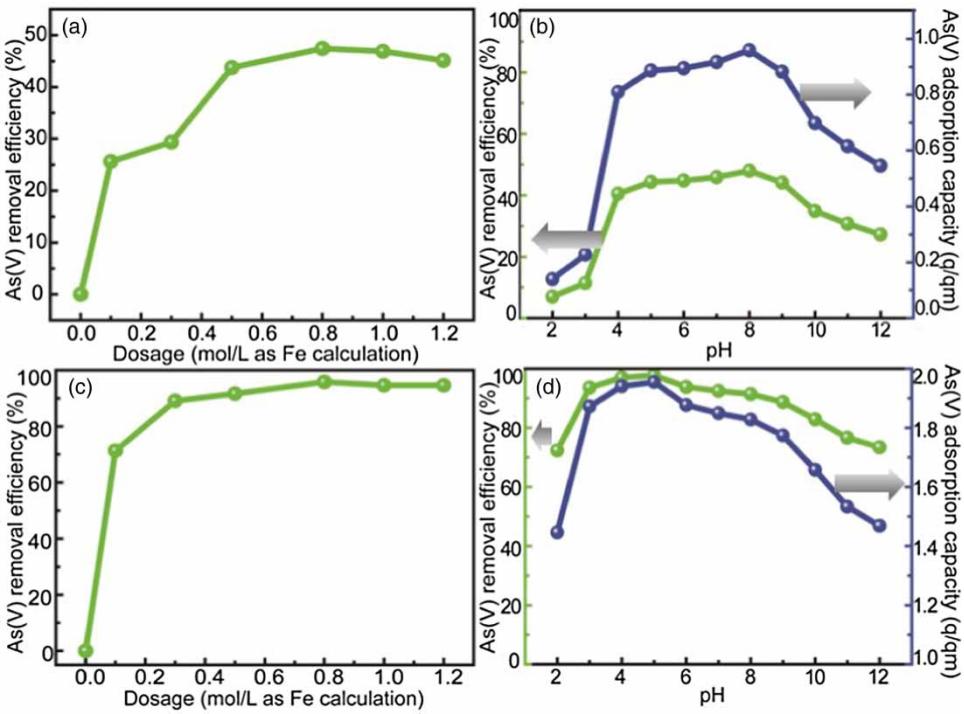

Figure 2 | (a) The effect of dosage on As(V) removal efficiency over granular activated carbon supported hydrated ferric oxide (Fe(III)) in the range from 0.1 mol/L to 1.2 mol/L as Fe calculation within initial As(V) concentration of 20 mg/L at pH 7.0. (b) The effect of pH in solution on As(V) removal efficiency and As(V) adsorption capacity over granular activated carbon supported hydrated ferric oxide (Fe(III)) in the range from 2 to 12 within initial As(V) concentration of 20 mg/L and adsorbent concentration of 0.8 mol/L as Fe calculation. (c) The effect of dosage on As(V) removal efficiency over granular activated carbon supported hydrated ferric oxide (Fe(II)) in the range from 0.1 mol/L to 1.2 mol/L as Fe calculation within initial As(V) concentration of 20 mg/L at pH 7.0. (d) The effect of pH in solution on As(V) removal efficiency and As(V) adsorption capacity over granular activated carbon supported hydrated ferric oxide (Fe(II)) in the range from 2 to 12 within initial As(V) concentration of 20 mg/L and adsorbent concentration of 0.8 mol/L as Fe calculation.

pH range from 3.0 to 9.0, indicating that other adsorption channels may exist. Therefore it is necessary to make in-depth investigations for adsorption mechanisms.

Thermodynamics

The effect of temperature on the adsorption of As(V) onto Fe(II)-GAC was carried out in the temperature range from 25 to 45 °C. The results indicated that the adsorption process is endothermic in nature. The equilibrium partition coefficient (Kc) is calculated as follows:

$$Kc = Cs/Ce \quad (1)$$

The thermodynamic parameters such as change in free energy (ΔG), enthalpy (ΔH) and entropy (ΔS) were calculated from the following equations and listed in Table 2.

$$\Delta G = -RT \ln Kc \quad (2)$$

$$\ln Kc = \Delta S/R - \Delta H/RT \quad (3)$$

where R is the gas constant (8.314 J/mol K), Cs and Ce are the equilibrium concentrations of the arsenic in the adsorbent (mg/L) and solution (mg/L), respectively, and T is the solution temperature (K).

ΔH and ΔS were calculated from the slope and intercept of the plot of lnKc versus 1/T. Relative thermodynamic parameters are presented in Table 2. The negative values of ΔG indicate that the adsorption of arsenic onto Fe(II)-GAC occurs spontaneously, while the positive values of ΔH suggest an endothermic process. The more negative values of ΔG imply a greater driving force to the adsorption process. The values of ΔH (46.3 kJ/mol, ranging from 8.4 kJ/mol to 83.7 kJ/mol) are high enough to ensure the strong interaction via chemical adsorption between the arsenate ions and the Fe(II)-GAC (Smith 1981). The positive values of ΔS indicate that the randomness increased at the solid-solution interface during the adsorption process.

Table 2 | Thermodynamic parameters for the adsorption of As(V) onto Fe(II)-GAC and Fe(III)-GAC

	T (K)	ΔG^0 (kJ·mol^{-1})	ΔS^0 [J·(mol·K^{-1})]	ΔH^0 (kJ·mol^{-1})	R^2
Fe(II)-GAC	298	−19. 296	216.580	46. 317	0.931
	308	−20.556			
	318	−22.828			
Fe(III)-GAC	298	−10. 935	77.686	12.695	0.992
	308	−11.432			
	318	−11.976			

Mechanisms

As discussed above, charge neutralization is not the only critical factor determining the better performance of Fe(II)-GAC. The As removal rate of Fe(II)-GAC is also found to be twice that of Fe(III)-GAC at the same dosage, especially in neutral conditions. Such unexpected results indicate that an alternative mechanism might exist, based on the confirmation of significant interaction between the matrix and HFO discussed above. Herein, As3d and Fe2p spectrums of XPS are adopted as explanations for adsorptive behaviors (Figure 3). The As3d spectrums of adsorbed Fe(II)-GAC exhibit peaks at 45.79 eV, which are higher than the As3d spectrums of Na_2HAsO_4•$7H_2O$ exhibiting peaks at 44.6 eV, reported by Chakraborty *et al.* (2011), indicating charge density imparted over the As atom. Meanwhile, the peaks of Fe2p and O1s shift from 711.87 and 532.06 to 711.69 and 532.03, respectively, demonstrating the enhancement of charge density over the Fe and O atoms. Therefore, the As adsorption mechanism may be ascribed to the charge transfer among Fe, O, and As. In detail, the charge transfer is induced by a lone pair of electrons in the outermost layer of As and Fe3d6 electrons configuration. It is known that the state of 3d6 is less stable than that of half-filled 3d5. Moreover, in order to minimize the total energy, external charge tends to take up 3d6 to form pairs of electrons with opposite spin direction. Therefore, it means that Fe(II) plays a role of electrons acceptor compared with neighboring atoms. Genuchten *et al.* (2012) also reported that the absence of corner-sharing FeO_6 octahedra could efficiently bind arsenic. Therefore, As species easily take up corners of FeO_6 octahedra. In this case, due to electrons-rich ions, As(V) acts as an electron donor. Therefore, charge transfer from As to Fe over O mediates not only red–shift as the XPS data demonstrated, but will also facilitate the adsorption process.

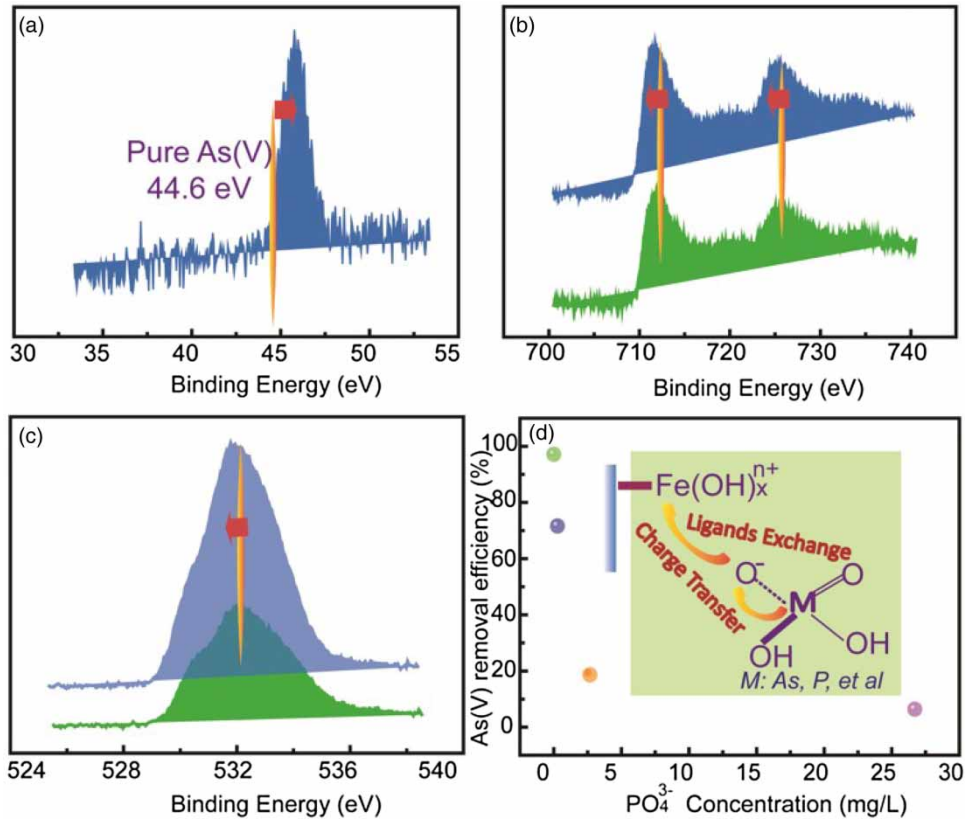

Figure 3 | X-ray photoelectron spectroscopy (XPS) spectrums of granular activated carbon supported hydrated ferric oxide (Fe(II)) before and after adsorption (Illustrated by arrow) with an Al Kα anode (1,486.6 eV photon energy, 0.05 eV photon energy resolution, 150 W). (a) As3d spectrum, (b) Fe2p spectrum, and (c) O1s spectrum. (d) The relationship between As(V) removal efficiency and interfering ion concentration and the illustrations of As(V) removal mechanism by granular activated carbon supported hydrated ferric oxide (Fe(II)).

To validate the mechanism proposed above, PO_4^{3-} is selected as a control sample for further experimental investigations. It is known that phosphorus shares the same electronic configuration as As, except for the atomic radius, due to the fact that it belongs to the same main group. Meanwhile PO_4^{3-} is also a typical organic pollutant in groundwater. Therefore, investigation of the inhibitory effects of PO_4^{3-} on arsenic removal and the corresponding mechanism will be necessary for the groundwater clean-up. Theoretically, the removal mechanism of PO_4^{3-} should be the same as that of As, depending on the similarity of the electronic structure. However, due to a smaller atomic radius, PO_4^{3-} can interact relatively easily with HFO because of weak steric hindrance effects, thus facilitating the adsorption process. Ultimately, more adsorptive sites will be taken up by PO_4^{3-}. Therefore, PO_4^{3-} has an inhibitory effect on arsenic removal as a result of charge transfer between Fe, O, and P.

Additionally, the inhibitory effects induced by other common inorganic ions in groundwater were also studied. The ions Na^+, Mg^{2+}, Ca^{2+}, F^-, Cl^-, NO_3^-, CO_3^{2-}, SO_4^{2-}, and SiO_3^{2-} were selected, and the corresponding inhibitory effect was measured by As(V) removal via tuning the molar ratio between inorganic ions and As(V) to 1:1, 10:1, 100:1, and 1,000:1, representing 0.267, 2.67, 26.7, and 267, respectively, in Figure S2 (Supplementary Material). As displayed in Figure S2, most of the co-existing ions (such as Na^+, Mg^{2+}, Ca^{2+}) showed almost no inhibitory effect on the adsorption of As(V), even at high concentrations. To some extent, such cations accelerate the adsorption ability resulting from narrowing the adsorption double layer. This performance may be ascribed to the fully filled s or p orbits, resulting in imparting electron transfer. However, the presence of CO_3^{2-}, SiO_3^{2-} and PO_4^{3-} species shows a severe inhibitory effect, which may be caused by their similar electronic configuration with proper energy level.

Compared with PO_4^{3-}, CO_3^{2-} could take up PO_4^{3-} adsorption sites because of the diagonal principle, but, due to the lack of an extra lone pair of electrons, the role of electron donor from carbon will be eliminated. For SiO_3^{2-}, although belonging to the same main group as carbon, Si still cannot play the role of electron donor. However, the energy gap of Si between 3p and 3d (highest occupied molecular orbits and lowest unoccupied molecular orbits), which is the same as that of phosphorus, is narrower than that of carbon, indicating that electrons are accepted from adjacent heteroatoms. Therefore, the order of inhibition as to the effects of co-existing ions on As(V) removal, no matter what kind of adsorbents, follows the sequence of $PO_4^{3-} > SiO_3^{2-} > CO_3^{2-} > F^- > NO_3^- \approx Cl^- \approx SO_4^{2-} > Na^+ > Mg^{2+} > Ca^{2+}$, further confirming the charge transfer mechanism of Fe(II)-GAC during the As(V) removal process.

CONCLUSIONS

In this article, the heavy metals adsorption capacity was found to be effectively tuned by controlling the electronic configuration of intrinsic adsorptive sites. Taking As(V) as the model component, electron transfer takes place over the Fe-O-As due to electron acceptors from empty bonding orbits of transition metals, and electrons donated from the As atom. With the same mechanism, PO_4^{3-} also proves the validity of the charge transfer channel. Therefore, based on this conception, the As(V) removal by Fe(II)-GAC is higher than that by Fe(III)-GAC even with a wider pH range. Collectively, this method will supply fundamental information for adsorbents design either for heavy metals or organics removal.

ACKNOWLEDGEMENTS

This work is supported by the National Natural Science Foundation of China (21707023), New Faculty Start-Up Funding from Xiangtan University (18QDZ16), and Provincial Key Research and Development Plan of Hunan Province (2018SK2034, 2018SK2018).

COMPLIANCE WITH ETHICS GUIDELINES

All authors (K.T., J.X., J.S., and H.Z.) declare that they have no conflict of interest or financial conflicts to disclose.

SUPPLEMENTARY MATERIAL

The Supplementary Material for this paper is available online at https://dx.doi.org/10.2166/ws.2019.197.

REFERENCES

Chakraborty, S., Bardelli, F., Mullet, M., Greneche, J. M., Varma, S., Hrhardt, J. J., Banerjee, E. D. & Charlet, L. 2011 Spectroscopic studies of arsenic retention onto biotite. *Chem. Geol.* **281** (1–2), 83–92.

Chowdhury, S. R. & Yanful, E. K. 2010 Arsenic and chromium removal by mixed magnetite–maghemite nanoparticles and the effect of phosphate on removal. *J. Environ. Manage.* **91** (11), 2238–2247.

Council of the European Union 1998 Council Directive 98/83/EC of 3 November 1998 on the quality of water intended for human consumption.

Cui, J., Jing, C., Che, D., Zhang, J. & Duan, S. 2015 Groundwater arsenic removal by coagulation using ferric (III) sulfate and polyferric sulfate: a comparative and mechanistic study. *J. Environ. Sci. (China)* **32**, 42–53.

Cumbal, L. & Sengupta, A. K. 2005 Arsenic removal using polymer-supported hydrated iron (III) oxide nanoparticles: role of donnan membrane effect. *Environ. Sci. Technol.* **39** (17), 6508–6515.

Fox, D. I., Stebbins, D. M. & Alcantar, N. A. 2016 Combining ferric salt and cactus mucilage for arsenic removal from water. *Environ. Sci. Technol.* **50** (5), 2507–2513.

Genuchten, C. M. V., Addy, S. E. A., Peña, J. & Gadgil, A. J. 2012 Removing arsenic from synthetic groundwater with iron electrocoagulation: an Fe and As K-edge EXAFS study. *Environ. Sci. Technol.* **46** (2), 986–994.

Gu, Z., Fang, J. & Deng, B. 2005 Preparation and evaluation of GAC-based iron-containing adsorbents for arsenic removal. *Environ. Sci. Technol.* **39** (10), 3833–3843.

Hu, J., Lo, I. M. & Chen, G. 2004 Removal of Cr (VI) by magnetite nanoparticle. *Water Sci. Technol.* **50** (12), 139–146.

Jaiswal, V., Saxena, S., Kaur, I., Dubey, P., Nand, S., Naseem, M., Singh, S. B., Srivastava, P. K. & Barik, S. K. 2018 Application of four novel fungal strains to remove arsenic from contaminated water in batch and column modes. *J. Hazard. Mater.* **356**, 98–107.

Jang, M., Chen, W. & Cannon, F. S. 2008 Preloading hydrous ferric oxide into granular activated carbon for arsenic removal. *Environ. Sci. Technol.* **42** (9), 3369–3374.

Jing, W., Zhang, S., Pan, B., Zhang, W. & Lu, L. 2011 Hydrous ferric oxide–resin nanocomposites of tunable structure for arsenite removal: effect of the host pore structure. *J. Hazard. Mater.* **198** (2), 241–246.

Kam, S. Y. & Gregory, J. 2001 The interaction of humic substances with cationic polyelectrolytes. *Water Res.* **35** (15), 3557–3566.

Kartinen, E. O. & Martin, C. J. 1995 An overview of arsenic removal processes. *Desalination* **103** (1–2), 79–88.

Li, Y., Wang, J., Luan, Z. & Liang, Z. 2010 Arsenic removal from aqueous solution using ferrous based red mud sludge. *J. Hazard. Mater.* **177** (1–3), 131–137.

Li, S., Yang, Q., Yu, Z., Chen, F., Xie, T., Yao, F., Sun, J., Chen, J., Li, X. & Zeng, G. 2016 Adsorptive bromate removal from aqueous solution by commercial strongly basic resin impregnated with hydrated ferric oxide (HFO): kinetics and equilibrium studies. *J. Chem. Eng. Data.* **61** (3), 1305–1312.

McNeill, L. & Edwards, M. 1997 Predicting As removal during metal hydroxide precipitation. *J. Am. Wat. Wks Assoc.* **89** (1), 75–86.

Ministry of Health of the P.R. China 2006 *Standard for Drinking Water Quality*.

Naeem, A., Woertz, J. R. & Fein, J. B. 2006 Experimental measurement of proton, Cd, Pb, Sr, and Zn adsorption onto the fungal species Saccharomyces cerevisiae. *Environ. Sci. Technol.* **40** (18), 5724–5732.

Naeem, A., Saddique, M. T., Mustafa, S., Kim, Y. & Dilara, B. 2009a Cation exchange removal of Pb from aqueous solution by sorption onto NiO. *J. Hazard. Mater.* **168** (1), 364–368.

Naeem, A., Saddique, M. T., Mustafa, S., Tasleem, S., Shah, K. H. & Waseem, M. 2009b Removal of Co^{2+} ions from aqueous solution by cation exchange sorption onto NiO. *J. Hazard. Mater.* **172** (1), 124–128.

Pan, B., Qiu, H., Pan, B., Nie, G., Xiao, L., Lv, L., Zhang, W., Zhang, Q. & Zheng, S. 2010 Highly efficient removal of heavy metals by polymer-supported nanosized hydrated Fe (III) oxides: behavior and XPS study. *Water Res.* **44** (3), 815–824.

Shen, J., Zhao, H., Cao, H., Zhang, Y. & Chen, Y. 2014 Removal of total cyanide in coking wastewater during a coagulation process: significance of organic polymers. *J. Environ. Sci.* **26** (2), 231–239.

Smith, J. M. 1981 *Chemical Engineering Kinetics*. McGraw Hill, New York, pp. 225–263.

U.S.EPA 2002 *Implementation Guidance for the Arsenic Rule*. EPA report-816-D-02–005, Cincinnati, USA.

World Health Organization (WHO) 2011 *Guidelines for Drinking-Water Quality*, 4th edn (incorporating the first addendum), WHO, Geneva.

Yan, D., Gang, D. D., Zhang, N. & Lin, L. 2011 Iron oxide-coated GAC adsorbents: diffusion-controlled sorption of selenite. *Ind. Eng. Chem. Res.* **50** (4), 2214–2219.

Yan, D., Li, H. J., Cai, H. Q., Wang, M., Wang, C. C., Yi, H. B. & Min, X. B. 2018 Microscopic insight into precipitation and adsorption of As(V) species by Fe-based materials in aqueous phase. *Chemosphere* **194**, 117–124.

Yuan, Z. D., Zhang, G. Q., Ma, X., Yu, L., Wang, X., Wang, S. F. & Jia, Y. F. 2019 Rapid abiotic As removal from As-rich acid mine drainage: Effect of pH, Fe/As molar ratio, oxygen, temperature, initial As concentration and neutralization reagent. *Chem. Eng. J.* **378**, 122156.

First received 5 June 2019; accepted in revised form 11 December 2019. Available online 30 December 2019